Diamond machining of additively manufactured Ti6Al4V ELI: Newer mode of material removal challenging the current simulation tools

Neha Khatri [a,b,*], Borad M. Barkachary [c], Sachin Singh [d], K Manjunath [a,b], Nitish Chandra [e], Joe Armstrong [f], Anupam Agrawal [g], Saurav Goel [h,i,**]

[a] Department of Manufacturing Science & Instrumentation, CSIR-CSIO, Sector 30, Chandigarh 160030, India
[b] Academy of Scientific and Innovative Research (AcSIR), Ghaziabad 201002, India
[c] Department of Mechanical Engineering, Jorhat Institute of Science & Technology, Jorhat 785010, Assam, India
[d] Mechanical Engineering Department, Thapar Institute of Technology, Patiala, Punjab 147004, India
[e] GEM Polytechnic College, Aurangabad, Bihar 824121, India
[f] Polytec GmbH, Polytec-Platz 1-7, 76337 Waldbronn, Germany
[g] Mays Business School, Texas A&M University, College Station, TX, USA
[h] School of Engineering, London South Bank University, London SE1 0AA, UK
[i] Department of Mechanical Engineering, University of Petroleum and Energy Studies, Dehradun 248007, India

ARTICLE INFO

ABSTRACT

Single point diamond machining (SPDM) produces smooth machined surfaces that other production methods cannot match. While the mechanics of machining of cast alloys with SPDM is well-explored, the realm of SPDM for additively manufactured parts remains largely uncharted. This work reveals new insights into the surface generation process of an additively manufactured titanium alloy, specifically, a Ti6Al4V Extra Low Interstitials (ELI) alloy workpiece. Our examination of the chip morphology unveiled a distinct mode of chip removal, previously unrecorded in existing literature. During SPDM of additively made Ti6Al4V ELI workpiece, identification of numerous pores and discontinuities in the chips flowing on the tool rake face, indicating periodic intermittent cracking during the material's plastic flow was seen. To examine this phenomenon, a finite element analysis (FEA) model was developed. While the FEA model can well explain the machining mechanics and chip morphology of SPDM of cast Ti6Al4V ELI reported in the literature, it failed to describe the chip morphology that are obtained during machining of additively made workpiece in this work. This disparity underscores the need for innovative simulation approaches tailored for additively manufactured components. The experimental observations in this study highlight a unique form of chip formation in contrast to conventional Ti6Al4V alloy machining processes. At lower feeds, there was a presence of short, discontinuous chip formation with tearing at the outer periphery. Conversely, at higher feeds, a long, continuous ribbon-like chip formation was observed. In addition, some typical additive manufacturing defects appear on the machined surface and chips. Through optimisation of the SPDT parameters, a surface roughness (Ra) value of about 11.8 nm was achieved on additively manufactured Ti6Al4V ELI workpiece. This work provides a fresh perspective on the mechanics of SPDM for additively manufactured components, offering a stepping stone for subsequent studies.

1. Introduction

As the demand for high-precision components grows, understanding the mechanics of Single Point Diamond Machining (SPDM) for additively manufactured titanium alloys has become paramount. While

traditional manufacturing methods of titanium alloys are well-documented, the nuances of machining additively manufactured components remain less explored. This research delves into these intricacies, shedding light on previously uncharted domains of SPDM.

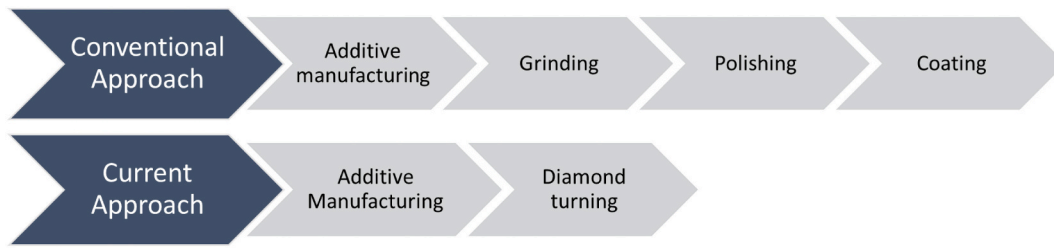Additive Manufacturing (AM) has demonstrated remarkable

Fig. 1. Conventional vs newly proposed sequential machining protocol to obtain finished machined parts of Ti6Al4V.

research potential across various domains, including biomedical implants, aerospace and defense applications, high-pressure cryogenic vessels and automobile components [1]. AM has revolutionized the manufacturing landscape by significantly reducing production costs and time [2]. For instance, producing a metal alloy such as titanium requires about 600 MJ/kg, resulting in over 36 kg of CO_2 emissions. Additionally, shaping the ingot through machining generates substantial material waste as cutting chips. The energy cost to remelt and transform these chips back into an ingot adds an extra 225 MJ/kg.

On the other hand, AM techniques such as Direct Energy Deposition (DED), Electron Beam Melting (EBM) and Selective Laser Melting (SLM) have attracted a significant research interest owing to its ability to produce near-net shape components at reduced expense of energy [3]. However, components fabricated using AM often do not meet the necessary surface quality standards without post-production processing and typically require additional machining. Fig. 1 illustrates and highlights the differences in conventional vs newer way of sequential machining that illustrates the potential to curb emissions while producing finished machined parts (such as the Ti6Al4V alloys).

SLM is one of the most popular AM techniques due to its numerous advantages such as unparallel degrees of design freedom, minimum surface defects and high reproducibility. SLM process has been explored by several researchers in the medical field for 3-dimensional (3D) printing of metallic medical implants and devices [4]. Titanium alloys made from Ti6Al4V Extra Low Interstitials (ELI) powder are an excellent choice for biomedical applications due to the low elastic modulus, higher strength, wear and corrosion resistance and biocompatibility [5]. However, the parts produced using SLM often exhibit high surface roughness (R_a) in the range of 2 μm to 40 μm [6]. While several factors contribute to this, the primary reasons seem to stem from high heat-induced heterogeneity in material recrystallization, limited control over the finishing process (attributed to the machines' varying degrees of freedom), suboptimal melting of powder particles, the balling phenomenon and the stair-step effect [2,7].

In the past decade, there has been a significant effort to understand the cutting mechanism of AM parts. For example, Hojati et al. [8] investigated the machinability of Ti6Al4V parts obtained from Electron Beam Melting (EBM), and noted that the uncut chip thickness plays a significant role in influencing the cutting forces in micro-milling. Ostara et al. [9] analyzed the machining of Inconel 718 obtained using Laser Metal Deposition (LMD), and specified that chip geometry is significantly different in terms of length and shape, i.e., chips were seen to be shorter and straight compared to those obtained from forged walls. Oyelola et al. [10] studied the machining behaviour and surface integrity of the Ti6Al4V alloy produced by Direct Metal Depostion, and obtained long stringy chip formation. Gael et al. [11] studied the machining behaviour and surface integrity of the Ti6Al4V alloy produced by Direct Metal Deposition and also noticed long stringy chips. Despite of these early efforts made, the poor surface finish (that can affect wear, corrosion, and fatigue performance of a part) constrains the range of precision engineering applications for which such parts are designed [12]. Moreover, an optimal surface finish is crucial in industries such as aerospace, automotive, and medical devices where component reliability and precision directly influence performance and safety.

Machining Ti alloys is often deemed challenging due to titanium's low thermal conductivity and high chemical reactivity, leading to rapid tool wear [13]. When it comes to the machining behaviour of cast Ti alloys, the formation of shear band-induced saw tooth chips is a well-documented phenomenon identified by various researchers. Most recently, the occurrence of brittle–ductile transition during diamond machining of ductile materials such as Ti alloys [14] has been reported. This behaviour is similar to what is seen inherently with nominal brittle materials such as SiC [15]. Colafemina et al. [16] demonstrated that the SPDM process is a viable option for finishing Ti alloy as it can achieve a peak-to-valley surface roughness, Rt ranging from 400 to 600 nm. Chauhan and Dass [17] studied the effect of process parameters (spindle speed, feed rate, approach angle and depth of cut) on the Ra of the Ti6Al4V (grade 5) workpiece. Their findings indicated a direct correlation between an increase in spindle speed and feed rate, and a rise in the workpiece Ra. Ramesh et al. [18] showed that feed rate during SPDM has the most significant effect on the Ra of the Ti6Al4V (grade 5) workpieces. Heidari and Yan [19] studied the cutting mechanism and chip formation behaviour during the SPDM of pure titanium and specified that flank wear, microchipping and material adhesion depends on the position of tool edge. Furthermore, if the undeformed chip thickness decreases down to critical value, chip edge tearing becomes significant. Zhang et al. [20] showed the effect of ultrasonic vibrations on diamond tool wear during SPDM of Ti alloy. Minton et al. [21] developed an internally cooled-diamond coated insert to inhibit the tool wear. Yip and To [22] integrated the eddy current during the SPDM of Ti alloy to reduce the tool-workpiece vibration which in turn reduced the diamond tool wear. The role of minimum quality lubrication (MQL) in combination with other machining parameters in influencing the machined surface roughness of Ti alloy workpiece and tool wear has also been reported [23].

Researchers have also reported numerical studies on machining of Ti alloys to verify the experimental results [24]. Most of these studies focus on conventional machining of cast Ti alloys. Obikawa and Usui [25] developed a FEM model to simulate the machining of Ti alloy with a cemented carbide tool for studying the chip formation, cutting temperature and mean cutting force and found a good agreement with the experimental results. Sekar et al. [26] carried out a numerical simulation of Ti alloy machining with titanium aluminium nitride coated tool to predict effective stress, strain, temperature, machining force, and chip morphology. Similarly, Styder et al. [27] reported a numerical study to evaluate induced residual stresses due the effect of different constitutive material models on machining of Ti alloy with an uncoated carbide tool. Hall et al. [28] combined numerical and experimental methodologies to discern the effects of the tool's rake angle on machinability of Ti alloy. The effect of different cutting tools on machining of Ti alloy was investigated experimentally and numerically [29]. Reddy et al. [30] found that the PCD tool is more effective compared to coated Carbide and CBN tool.

Studies on FEA simulation of SPDM of Ti alloys are few. Lou and Wu [31] performed numerical simulation of ultra-precision machining to study the machinability of Ti alloy before and after the electro-pulsing treatment (EPT). They observed that EPT techniques can improve the
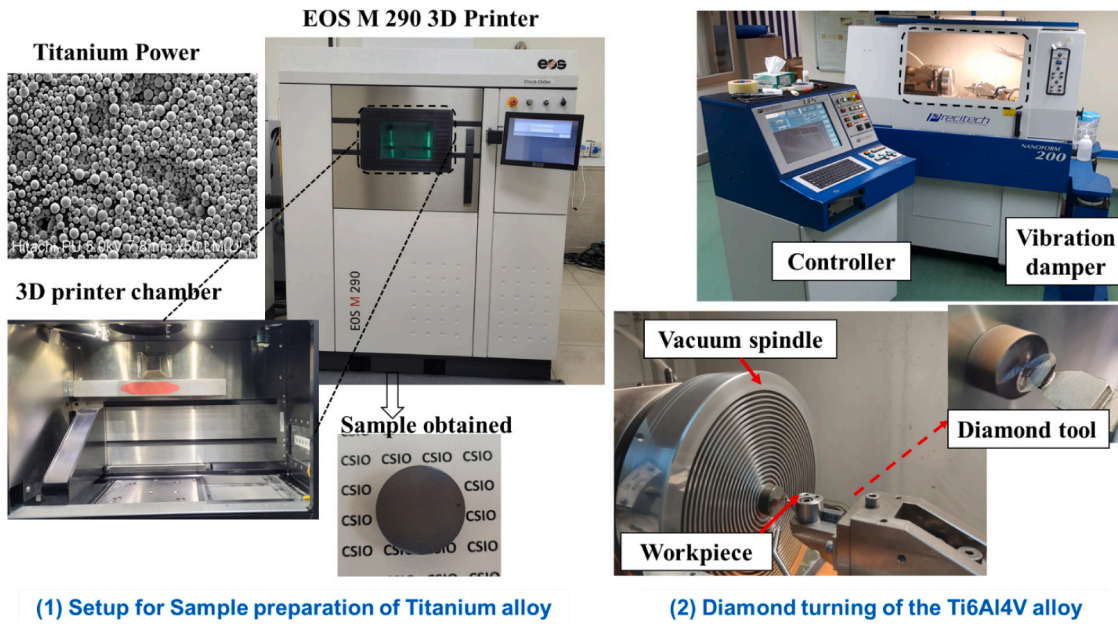
Fig. 2. Manufacturing protocol and sequence followed to fabricate the Ti6Al4V ELI alloy and its SPDM.

surface finish, lower the cutting forces and power spectral densities and this helps to obtain continuous chips. Amir et al. [32] reviewed various techniques and methodologies used in the development of FEA and suggested that material speration criteria is critical in getting accurate simulation results. Liu et al. [32,33] compared a wide range of reported consitutive models of Ti alloys using FEA and suggested that almost all the models can demonstrate saw-tooth chip formation mechanism, a behaviour consistently observed during machining of cast titanium alloys.

The literature indicates that SPDM of titanium alloy workpieces is limited [3], presenting a notable gap in the understanding of SPDM for additively manufactured titanium alloy workpieces. In the present study, a comprehensive experimental investigation on the SPDM of additively manufactured Ti6Al4V workpieces was undertaken. A series of machining trials was conducted using diamond tools with nose radii of 1 mm and 5 mm to gain insights into the cutting mechanism during SPDM of additively made Ti6Al4V ELI workpieces. Additionally, Finite Element Analysis (FEA) was employed to analyze cutting forces and chip formation using ABAQUS/Explicit® software. Experiments revealed a new chip formation mechanism. This novel chip formation, distinct from traditionally observed mechanisms in cast titanium alloys, hints at unique material behaviours during SPDM of additively manufactured alloys. A deeper dive into this phenomenon can revolutionize our understanding of machining dynamics and open new avenues for precision manufacturing of additively made alloys. These findings underscore the need for creating better computational models to more accurately capture the machining dynamics of additively manufactured titanium alloys.

2. Materials and methods

2.1. Additive manufacturing of the Ti6Al4V ELI samples

Fig. 2 shows a snapshot of the experimental protocol comprising additive manufacturing followed by diamond machining that was followed in this work. Details on the parameter optimisation for additively manufactured Ti6Al4V ELI alloy are available in prior publications, and as such, they are omitted here for brevity [34–36]. The selective laser melting (SLM) process was used for additive manufacturing of the Ti6Al4V ELI employing the 3D printing equipment: EOS M290 [36]. The

Table 1
Optimal process parameters to produce Ti6Al4V ELI using SLM process.

S. No	Printing parameter	Value
1.	Type of laser	Neodymium-doped yttrium aluminum garnet (Nd-YAG)
2.	Diameter of laser beam	80 μm
3.	Scanning velocity	1500 mm/s
4.	Layer thickness	30 μm
5.	Laser power	250 W
6.	Hatch spacing	0.2 mm

EOS M290 comes with a fibre laser with the maximum power of 400 W and wavelength of 1070 nm [35]. Various factors such as laser power, hatch space, and laser scan speed can influence the quality of additively manufactured part [37]. Furthermore, the properties of the powder are also critical in influencing the quality of the additively made part. The raw ingredient for this study, i.e., the Ti6Al4V ELI powder used was EOS titanium Ti6Al4V Grade 23. Its microscopic characterisation showed that the particle shapes were predominantly spherical with an average size of 37 μm [34,35].

Optimizing the parameters of the SLM process is crucial for achieving the desired mechanical and surface characteristics of the end product. The parameters of the AM manufacturing such as laser power, hatch space, and laser scan speed were optimised using Analysis of Variance (ANOVA) and Grey Relational Analysis (GRA) to obtain good mechanical and surface characterstics such as hardness and wear resistance. To achieve this, three levels of input parameters were considered for laser power as 250, 300 and 350 W, hatch space (mm) of 0.10, 0.15 and 0.20 mm and laser scan speed of 900, 1200 and 1500 mm/s. The minimum surface roughness obtained from these trials was about 0.585 μm whereas the worse roughness obtained was about 1.942 μm. The results from these trials showed that the increase in laser power can significantly reduce the surface roughness. Also, ANOVA showed that laser power is most influential (32.68 %) followed by hatch space (29.62 %) and laser scan speed (28.99 %) in achieving the additive part with superior mechanical finish. Such findings suggest that careful calibration of laser power, hatch space, and laser scan speed is essential for achieving a part with the best mechanical finish. A series of such trials led to the identification of the most optimal parameters as laser power of

Table 2

Mechanical properties of the additively manufactured Ti6Al4V alloy.

S. no	Mechanical properties	Value
1.	Bulk density	4.42 g/cc
2.	Yield strength	965 MPa
3.	Tensile strength	1071 MPa
4.	Young's modulus	110 GPa
5.	Layer thickness	30 μm

Table 3

Details of the diamond tool used.

S. no	Properties	Value
1.	Tool type	Monocrystalline
2.	Diamond crystal orientation	Dodec
3.	Clearance type	Conical
5.	Nose radius	1 mm and 5 mm
6.	Rake angle	0°
7.	Clearance angle	10°

250 W, laser scan speed of 1500 mm/s, hatch spacing of 0.2 mm, layer thickness of 30 μm and the built plate temperature as 35 °C [38] (see Table 1). The mechanical properties of the additively made Ti6Al4V ELI workpieces are specified in Table 2.

To prevent oxidation, the manufacturing process was carried out in an argon gas environment. Post SLM, all specimens were subjected to a heat treatment at 800 °C for 2 h [34]. They were then annealed to 300 °C for 4 h. The wirecut EDM process was then used to separate the Ti6Al4V ELI samples from the baseplate. A lapping process was performed to reduce the Ra value to be approximately 1–2 μm.

2.2. Diamond machining of the additively manufactured Ti6Al4V ELI samples

To achieve the required precision and surface finish for the additively manufactured Ti6Al4V ELI samples, diamond machining was employed. The process was carried out on a three-axis CNC contouring lathe machine (Model: Precitech Nanoform 200 ultra-precision). This machine comes with two perpendicular linear tables supported by high-stiffness hydrostatic bearings driven by servomotors. The linear tables can be moved at 1 nm per step and the rotary table has an angular resolution of 0.00001°. Such precision ensures high-fidelity machining suitable for complex and delicate structures. A sequence of operations performed as part of this work starting from the powder to the finished machined wafer is shown in Fig. 2.

The diamond machining in this study made use of a single-point diamond cutting tool (Contour Tooling, UK). The machining parameters were tested at three distinct levels:

- Spindle speeds: 2000, 3000, and 4000 rpm
- Feed rates: 1, 3, and 5 mm/min
- Depth of cut: 1, 5, and 10 μm

The experiments were conducted using two diamond cutting tools with nose radius of 1 mm and 5 mm respectively. Both cutting tools had the cutting edge radii of approximately ~150 nm, rake and clearance angles of 0° and 10° (see Table 3). This comprehensive setup, equipped with precise machinery and carefully selected parameters, aimed to achieve the best possible surface finish and mechanical properties for the Ti6Al4V ELI samples. The post-machining SPDM samples were assessed using non-contact detection techniques (widely utilized for 3D-surface roughness assessment), Coherence Correlation Interferometry of ×50 magnification (Taylor Hobson make) for evaluation of surface quality. The assessment of titanium chips and diamond tools involved the use of JSM-IT 100 In TouchScope™ Scanning Electron Microscopy (SEM) at 10 kV, employing various magnifications.

Table 4

ANOVA Results for Surface Roughness (Ra).

Source	DF	Partial SS	Mean square	F-value	P-value
Model	15	55,465.12	3697.67	130.88	0.0076
Tool Nose Radius (TNR)	1	326.56	326.56	11.56	0.0767
Spindle Speed (RPM)	2	4380.65	2190.33	77.53	0.0127
Feed Rate (FR)	2	41,350.32	20,675.16	731.81	0.0014
Depth of Cut (DoC)	2	1878.47	939.23	33.24	0.0292
FR x RPM	4	1290.51	322.63	11.42	0.0821
FR x DoC	4	2329.88	582.47	20.62	0.0468
Residual	2	56.5	28.25		
Total	17	55,521.62	3265.98		
R-squared = 0.9990, Adj R-squared = 0.9913					

To find the relative significance level of the SPDM process parameters and quantify their influences on the Ra, analysis of variance (ANOVA) was carried out as per the input details shown in the Supplemenatry information Tables S1 and S2.

Our experimental design comprising 18 experimental runs was based on Taguchi's L18 orthogonal array, which, while offering a comprehensive examination of the main effects and a selected subset of two-factor interactions, does not inherently support the examination of all possible interactions without extending beyond the constraints of the array. Given the complexity of the machining process, where factors such as nose radius, spindle speed, feed rate, and depth of cut interact in non-linear ways, this limitation is significant. Consequently, two specific interactions based on their significant theoretical and practical implications in machining: Feed Rate with Spindle Speed and Feed Rate with Depth of Cut were investigated. The interaction between spindle speed and feed rate is crucial for understanding the cutting conditions that directly influence the machined surface's quality. Similarly, the interaction between feed rate and depth of cut plays a pivotal role in determining the material removal rate and, by extension, the surface finish (Table 4).

The ANOVA analysis revealed that the model is significant (overall $p = 0.0076$), demonstrating the collective effect of the factors under study on surface roughness. Among the main effects, spindle speed and feed rate are statistically significant, with $p = 0.0127$ and $p = 0.0014$, respectively, highlighting their critical roles in determining Ra. Depth of cut also showed a significant influence on Ra ($p = 0.0292$). The impact of tool nose radius on Ra is not statistically significant. The interaction terms, including feed rate with spindle speed and feed rate with depth of cut, do not reach statistical significance, suggesting that their combined effects on surface roughness do not significantly deviate from the individual effects under the conditions tested. The residual analysis indicates a good model fit, with minimal unexplained variability, underscoring the importance of feed rate, spindle speed, and depth of cut in influencing the machining process's surface finish. The model has high explanatory power, evidenced by an R^2 value of 0.9990 and an Adjusted R^2 of 0.9913, indicating that nearly all variance in surface roughness is effectively accounted for by our selected factors and their interactions. This highlights the robustness of our experimental design and the relevance of our findings.

3. Machining results from SPDM

3.1. Surface roughness

Surface roughness is one of the most industrially prominent parameters used to evaluate the surface quality of a machined wafer. In order to measure the 2D surface roughness, a contact type (stylus based) Phase Grating Interferometer (Taylor Hobson make) was utilized. Fig. 3(a) shows the roughness of the machined workpiece with an initial Ra value of 1.98 μm. The Ra of this initially printed specimen was reduced down to <1 μm using the lapping method (see Fig. 3(b)). After performing
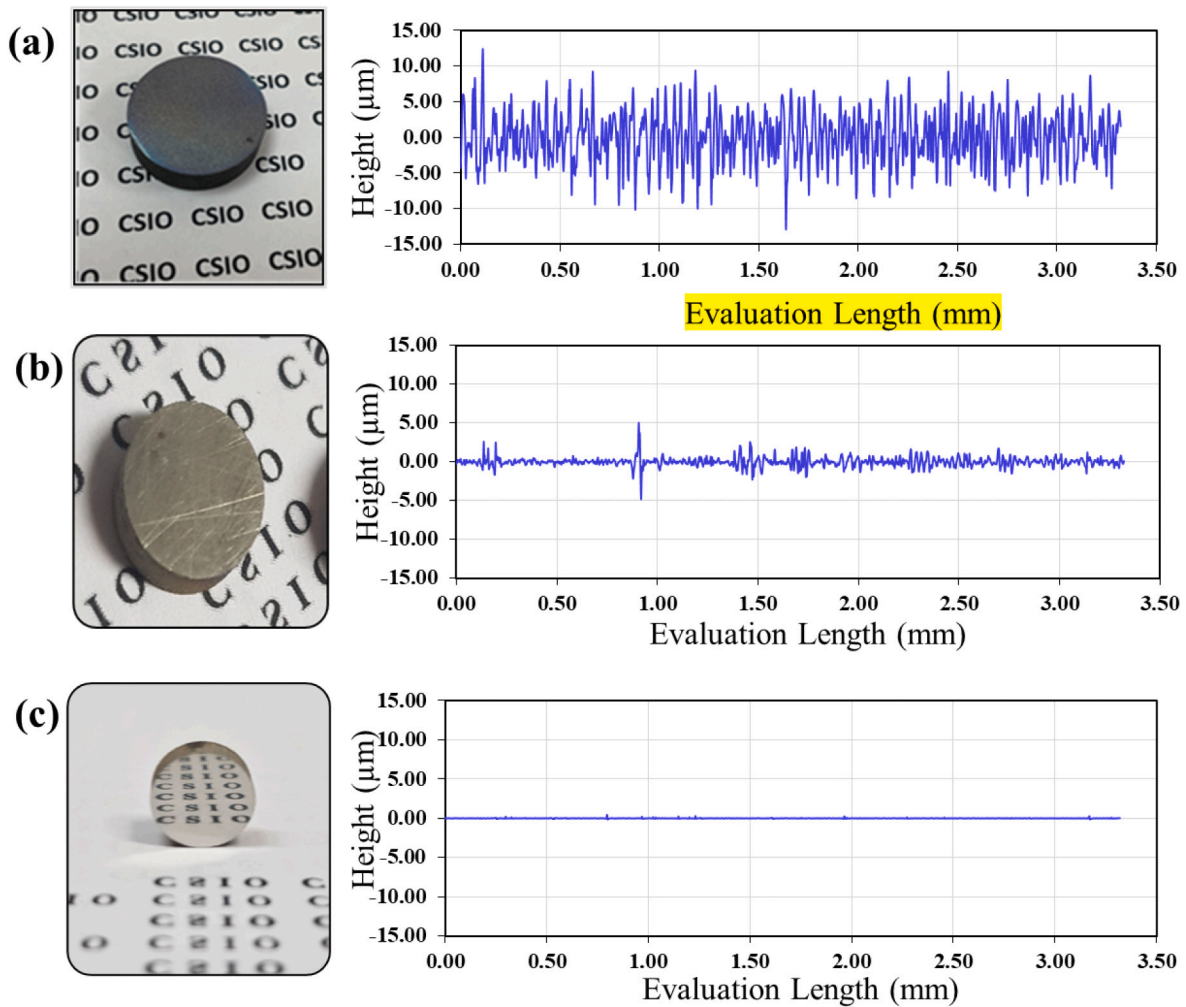
Fig. 3. Workpiece surface with corresponding 2D surface roughness profile (a) as additively manufactured sample (b) lapped sample and (c) diamond turned sample.

SPDM on the lapped samples using the optimum process parameters with a 1 mm nose radius diamond tool at a spindle speed of 2000 RPM, feed of 5 mm/min and depth of cut of 10 μm, a mirror-finished surface roughness with an Ra of 11.81 nm was obtained (Fig. 3(c)).

To review the influence of the machining parameters on the surface roughness, a detailed investigation was carried out. The relationship between feed rate and surface roughness in machining processes is generally direct; increasing the feed rate often increases the surface roughness. In the case of diamond turning of cast Ti alloys, this relationship holds. However, during the diamond machining of additively manufactured Ti6Al4V, a unique phenomenon was observed: an increase in feed rate led to a decrease in surface roughness. This observation deviates from the conventional wisdom in machining. One possible explanation for this phenomenon is that, at lower feed rates, the ploughing effect dominates the micro-cutting mechanism rather than the shear effect at lower feed rates [7].

The surface roughness (Sa) plots obtained from optical profiler coherence correlation interferometer (CCI) at 50× magnification for two feeds of 1 mm/min and 5 mm/min are shown in Fig. 4. The experimental results shown in Fig. 4(a) and (b) demonstrate that a feed rate of 1 mm/min yields a poor machined surface (with an average roughness of 152.67 nm) while a feed rate of 5 mm/min produces a smooth surface with an average surface roughness of 13.86 nm. This unusual relationship between feed rate and surface roughness represents a substantial departure from traditional machining processes, underscoring the distinct nature of diamond machining for additively manufactured

materials. This unique result could be ascribed to the fact that an increase in the feed rate decreases the track length (length of the tool path) and number of contact points along the machining length. With fewer contact points and shorter track lengths, the tool experiences reduced wear over time, leading to superior surface finishes. Additionally, when examining the effect of spindle speed on surface roughness, it was observed that lower spindle speeds yield better surface quality in comparison to higher spindle speeds. Another interesting observation was made when varying the tool nose radius between 1 mm and 5 mm, it was noticed that the 1 mm nose radius tool produced better surface quality. To better understand this phenomenon, detailed studies were conducted on tool wear characteristics and chip morphology, which will be discussed in the following sections.

Fig. 4(c) is a sample of the stiched measurement obtained from the Polytec profilometer to highlight and depict the quality of machining on the entire Ti6Al4V ELI sample. The process of generation of a stiched image to show the roughness across the entire sample is a time consuming process which requires accuracy of the instrument and skills of metrology to generate an image stitching progamme. Fig. 4(c) thus provides a high degree of confidence in the quality of equipment used for machining and metrology in this work. It also indicated that the unique observations reported in this work cannot be ascribed to the faulty instruments or the setup used in the experiments.
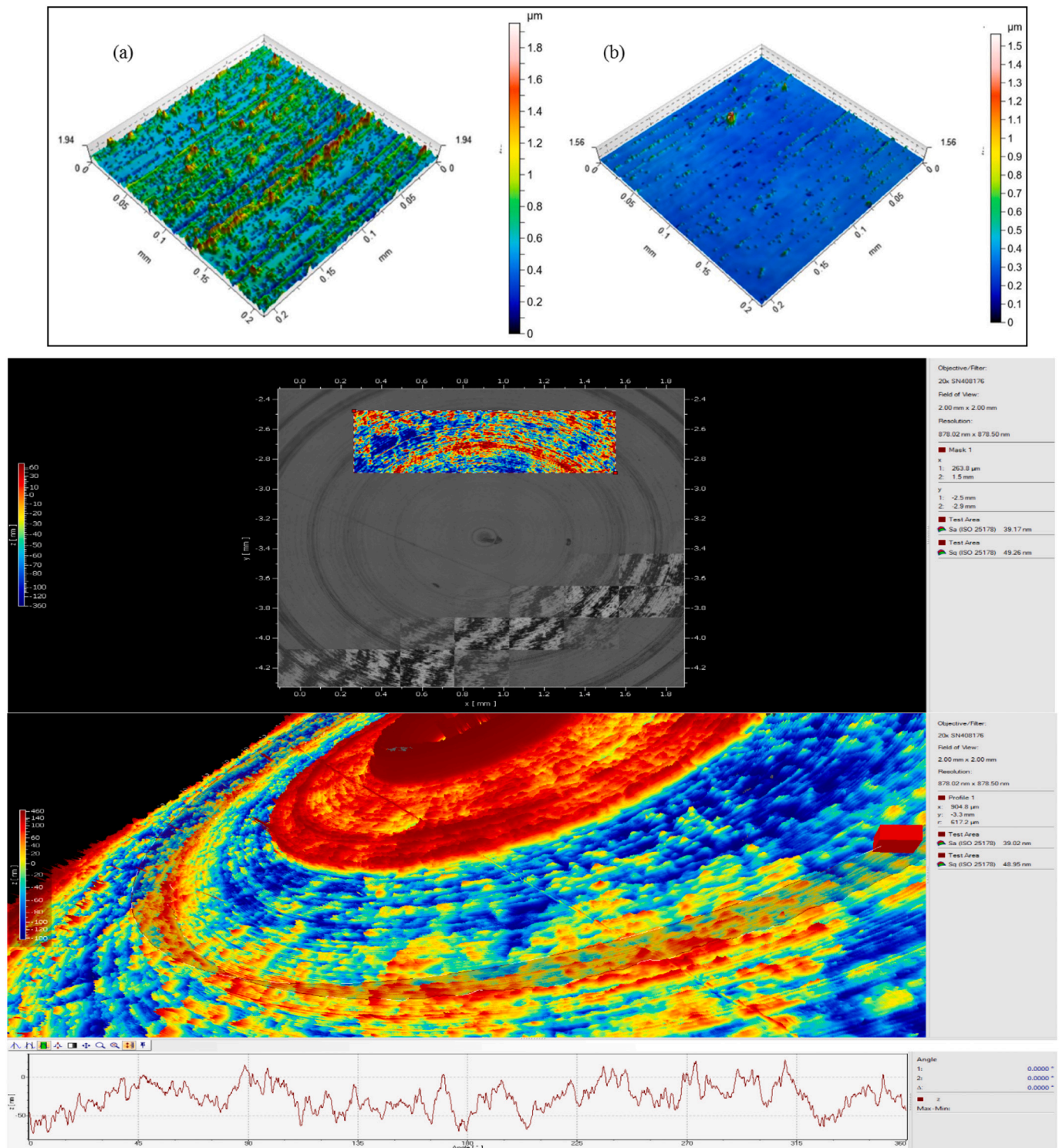
Fig. 4. 3D surface morphology obtained after diamond turning of additively manufacture titanium alloy at feed rates of (a) 1 mm/min and (b) 5 mm/min (c) Stiched profilometer image of the entire Ti6Al4V sample after its processing.

3.2. Discussion on chip morphology

A key component in understanding the SPDM of Ti6Al4V is the examination of chip morphology. The morphological patterns of chips can unveil new insights into the cutting process and offer clues about process efficiency, tool wear and resultant surface quality. The chip morphology of the cut chips produced from the SPDM process were examined using the SEM. The analysis of chip morphology revealed serration, primarily

due to the adiabatic shear [39] which are commonly reported in literature. During cutting of SLM made Ti6Al4V ELI parts, different type of chip morphology was observed. This distinctive chip formation can be ascribed in parts to the steep temperature gradients and high cooling rates during SLM process [39].

Feed rate played a crucial role in dictating chip morphology. At a feed rate of 5 mm/min, the chip pattern appeared porous, long, and continuous ribbon type as depicted in Fig. 5 (a). Such morphological
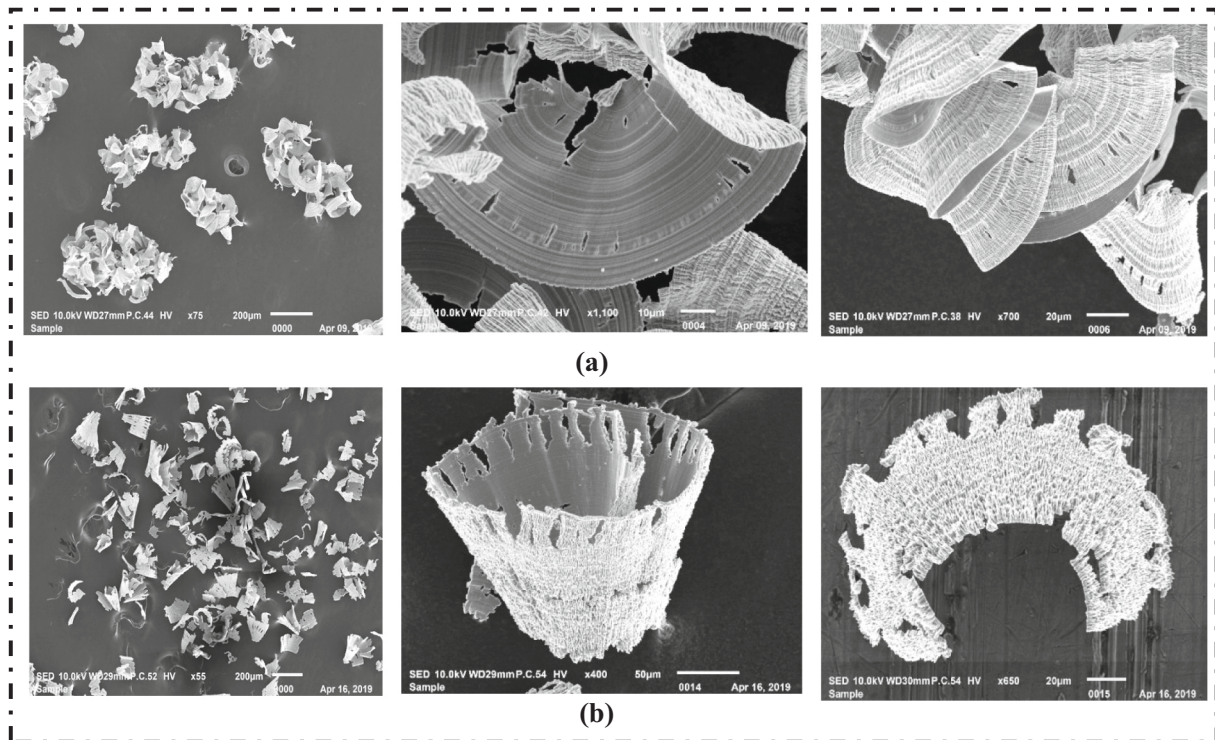
Fig. 5. Chip morphology obtained at feed rates of (a) 5 mm/min (b) 1 mm/min.
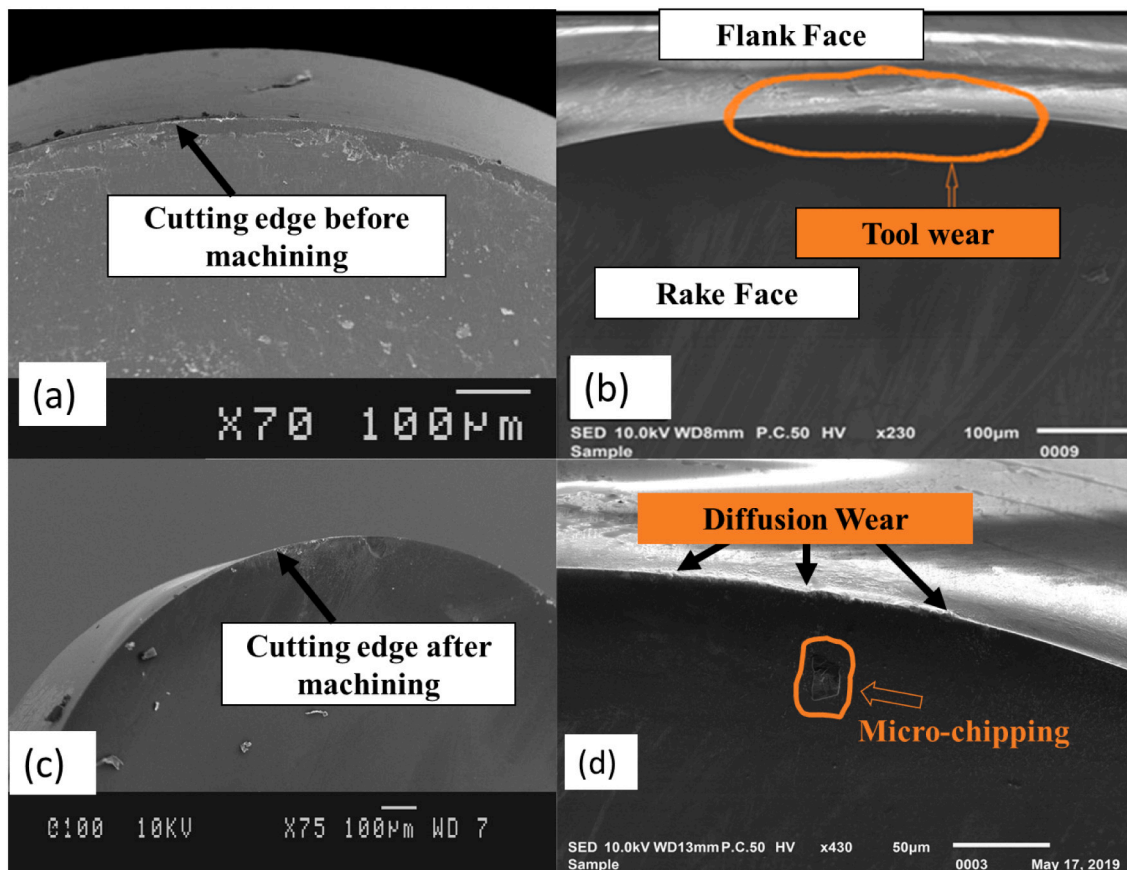

Fig. 6. SEM examination the diamond tool with 1 mm tool nose radius (a) Pristine cutting edge before machining (c) Tool wear after a cut distance of 100 m. Zoomed view of the (b) Cutting edge (d) Diffusion wear and micro chipping of the tool.
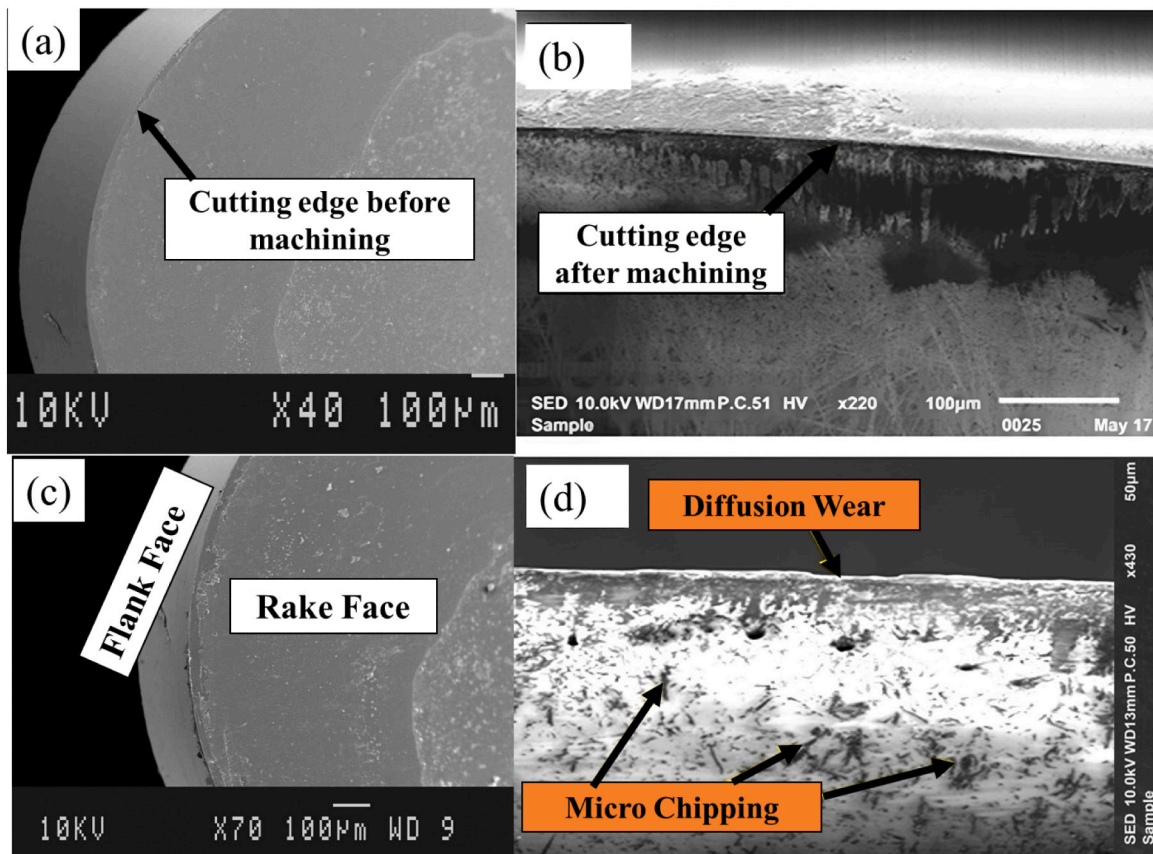
Fig. 7. SEM examination the diamond tool with 5 mm tool nose radius (a) Pristine cutting edge before machining (c) Tool wear after a cut distance of 100 m. Zoomed view of the (b) Cutting edge (d) Diffusion wear and Micro chipping on tool.

patterns in the generated chips are typically indicative of consistent, uniform material removal during the cutting process. At high feed rate, the tool-chip contact surface is smooth with some sliding marks leading to continuous ribbon chip formation. On the other hand, at a low feed rate of 1 mm/min, the chips were seen to be shorter in shape and discontinuous types accompanied by tearing on the outer periphery as shown in Fig. 5(b). At low feed, the compressive stress leads to the coverage of the chip with many extruded striped textures which leads to torn-off from both edges resulting in shorter chip formation. In both these cases, the chips can be seen to have holes in the centre – a very unique phenomenon observed in the history of machining chips of Ti alloys. It may also be noted that some undesired chips appeared at the edge of chips; this is moreover due to some defects (voids) during additive manufacturing, tool-tip vibration [40] and partly also due to the material recovery behaviour [41]. Furthermore, these defects (broken chips and debris) become more prominent with an increase of the feed rate due to the friction and extrusion caused by the local plastic deformation [42].

3.3. Discussion on tool wear

The role of diamond tools with different radii was examined by analysis of the diamond tool wear of the two tools at varying cutting distances. Figs. 6 and 7 show the SEM micrographs of the diamond tool cutting edges after cutting of Ti6Al4V ELI material with 1 mm and 5 mm tool nose radii respectively. The 1 mm nose radius showed reduced material adhesion on the tool face (compared to the tool with the 5 mm nose radius). It may be caused by the lower contact pressure at the tool-workpiece interface. Further, some micro-chipping on the rake face and diffusion wear on the tool tip face was also noticed after a cutting distance of 100 m under dry conditions (no coolant). This is due to the

diffusion process where atoms in a crystal lattice move from a region of high concentration to low concentration, which further weakens the surface of the cutting tool and leads to tool failure. The extent of diffusion depends on the cutting temperature, the binding affinity between the tool material and chip, the solubility of the tool in work material, and the period of contact between the tool and the chips. The favourable condition for diffusion is provided by the localized high temperature at the tool-chip interface.

The material adhesion on tool sharply increases with the 5 mm nose radius as compared to the 1 mm nose radius. Fig. 6 shows diffusion wear, built-up-edge, micro chippings and adhered titanium particles on the rake face of diamond tool with the larger nose radius. The figure indicates that more pores were closed due to higher pressure induced by the dull tool tip during the cutting process. As a result, tool wear increases due to the highly localized stress and strong adhesion at the tool-chip interface (rake & flank face) close to the tool cutting edge. At the same time, built-up edges are found on the rake face and small flank wear lands along with a few micro chippings which are observed around the tool edge. Our exploration into chip morphology and tool wear reaffirms the complex relationship between tool geometry, machining parameters, and the resultant machining quality.

4. FEA simulation of cutting of Ti6Al4V alloy using traditional constitutive model

Abaqus® software was used to simulate the cutting of Ti6Al4V to understand different aspects of chip morphology and cutting forces. The model used was the 3D stress dynamic explicit Arbitrary Lagrangian-Eulerian (ALE) solver. The objective was to first validate it with the prior published experimental results on diamond machining of cast titanium alloy and then to use the validated model to simulate the results
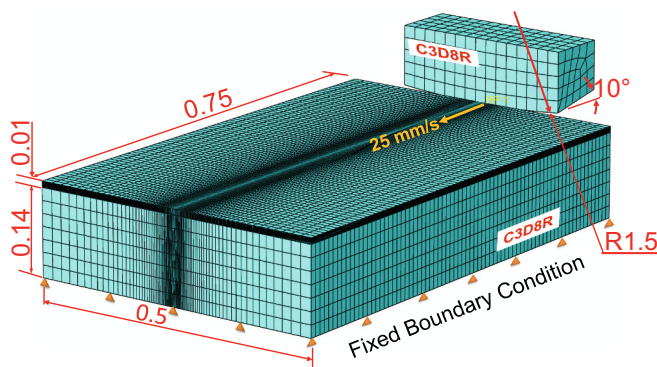
Fig. 8. CAD geometry showing the workpiece and the tool to mimic the previously published experimental results on cast Ti6Al4V alloy [14].
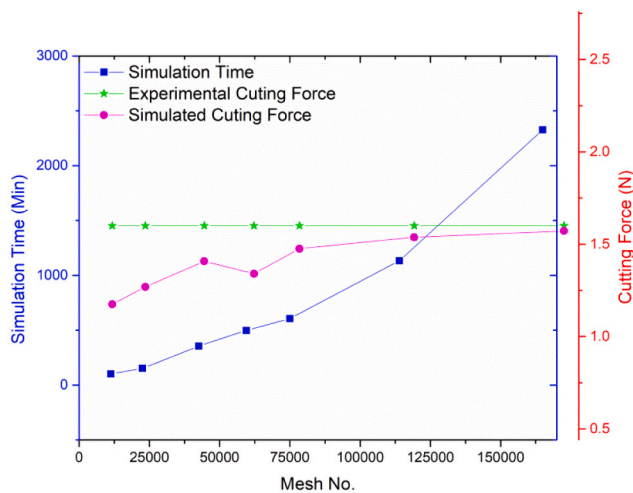
Table 5
Mechanical and thermal material properties of diamond [44] and Ti6Al4V [45].

Parameters	Unit	Diamond	Ti6Al4V
Density (ρ)	Kg/m^3	3350	4430
Young's modulus (E)	GPa	1000	109 (50 °C)
			91 (250 °C)
			75 (450 °C)
Poison's ratio (υ)		0.07	0.34
Thermal conductivity (k)	W/m.K	700	6.8 (20 °C)
			7.4 (100 °C)
			9.8 (300 °C)
			11.8 (500 °C)
Thermal expansion (α)^a	10^{-6}/K	4.0	8.6 (20 °C)
			9.2 (250 °C)
			9.7 (500 °C)
Specific heat (C)	J/kg.K	520	611 (20 °C)
			624 (100 °C)
			674 (300 °C)
			703 (500 °C)
Melting point (Tm)	°C	4373 @125 kbar	1560

^{a} asm.metweb.com

Fig. 9. Mesh sensitivity analysis to adjust the FEA solver parameters.

Table 6
J-C constitutive material model parameters of Ti6Al4V [46].

A [MPa]	B [MPa]	C	n	m
860	683	0.035	0.47	1.0

Table 7
J-C constitutive damage parameters [47].

d1	d2	d3	d4	d5
−0.09	0.25	−0.5	0.014	3.85

found in the current experimental setup (i.e., the additively manufactured Ti6Al4V ELI alloy workpiece). The model was an expansion of a previous work [43], therefore, most assumptions, material behaviour, element type, mesh schemes, contact properties and solver settings were kept similar. Further details of the FEA model development are discussed below.

4.1. Description of the FEA model to validate baseline results reported in literature

A schematic of the FEA model of the cutting process considering the effects of nose radius is shown in Fig. 8. The 3D rectangular workpiece was created with dimensions of 0.75 × 0.5 × 0.15 mm. The diamond tool with a 0° rake angle and a 10° clearance angle with a nose radius of 1.5 mm was modelled. For the comparative study, three process conditions with varying depth of cuts 2 μm, 4 μm and 7 μm were considered to simulate the experimental conditions reported by Yip and To [14]. To reduce the simulation time, the cutting speed was scaled up by a factor of ten, leading to a simulated speed of 25 mm/s. The bottom of the workpiece was kept fixed by clamping the workpiece. The common simplifying assumptions were considered such as (a) the workpiece material is isotropic and homogeneous as the machining simulation was carried out only in one direction for a small length, (b) the workpiece material is free from initial internal residual stresses and elastic-plastic type, and (c) The cutting length considered in the simulation was just 0.75 mm for which tool wear was neglected and modelled as rigid body. FEM can simulate the chip separation naturally without introducing any

physical, geometrical separation criteria. Modified Coulomb friction model was defined to represent the contact between the cutting tool and the workpiece with coefficient of friction of 0.24.

A general-purpose eight-node linear brick element C3D8R with reduced integration, hourglass control and element deletion (for workpiece) was used to mesh the tool and the workpiece geometry. The cutting region was prescribed a fine meshing whereas the region away from cutting was prescribed coarser meshing. An extensive set of FEA trials (mesh sensitivity analysis) were carried out to find the optimal mesh size. The key result from this analysis shown in Fig. 9, shows that the value of the simulated cutting force converges with the experimental cutting force at an instance when the Mesh size was about 165,000. Hence, for the current study, 165,000 mesh elements were considered.

The mechanical and thermal properties of Ti-alloy and diamond tool used in the simulation are listed in Table 5. To simulate the Ti-alloy's material response, Johnson and Cook (J-C) constitutive model, with parameters as outlined in Tables 6 and 7 were used.

4.2. Numerical results and discussions

Our FEA simulation work is organized into two distinct stages:

(a) Model Validation with Published Data: In the initial stage, we adjusted the cutting parameters in our FEA model to replicate previously documented results on the cutting of cast Ti6Al4V alloys. This stage helped to validate our simulation framework against established results.

(b) Simulation for SPDM of Additively Manufactured Parts: With the model validated, we then modified the cutting parameters to reflect the Single Point Diamond Machining (SPDM) conditions for additively manufactured components. Comparing these predictive FEA outcomes with our newly acquired experimental

Table 8

Comparison of simulated and experimental chip profiles for 2 μm, 4 μm and 7 μm depth of cuts (DOC) obtained for the machining of cast Ti6Al4V alloy workpiece.

Machining conditions	Chips obtained from experiments on cast Ti6Al4V alloy published by Yip and To [14]	Chips obtained from the FEA simulation in this work
Combination 1: Speed: 25 mm/s, TFR: 0 mm/s, DOC: 2 μm		
Combination 2: Speed: 25 mm/s, TFR: 0 mm/s, DOC: 4 μm		
Combination 3: Speed: 25 mm/s, TFR: 0 mm/s, DOC: 7 μm		

Table 9

Comparison of simulated and experimental chip widths for 2 μm, 4 μm and 7 μm depth of cut obtained after the machining of cast Ti6Al4V alloy workpiece.

Combinations	Experimental chip width	Simulated chip width	Analytical chip width
Combination 1: Speed: 25 mm/s, TFR: 0 mm/s, DOC: 2 μm			109.25 μm
Combination 2: Speed: 25 mm/s, TFR: 0 mm/s, DOC: 4 μm			154.40 μm
Combination 3: Speed: 25 mm/s, TFR: 0 mm/s, DOC: 7 μm			204.05 μm

results, we noticed discrepancies between the simulated and actual data, which we'll delve into in the subsequent discussions.

4.2.1. Validation of numerical model with published results on cutting of cast titanium alloys
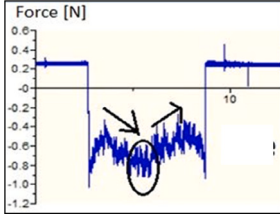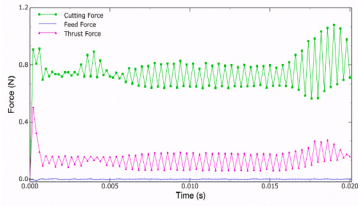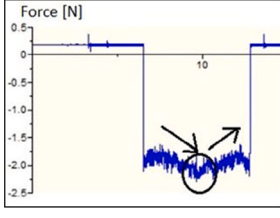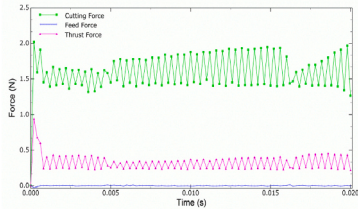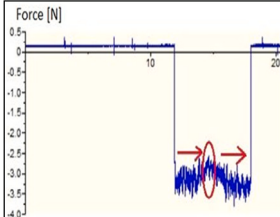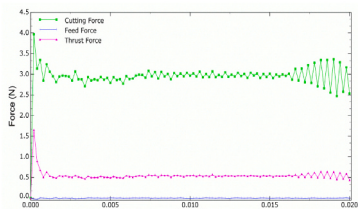
For validating the FEA model, a comparison was made between our simulation outcomes and the published experimental results. The machining outputs such as chip morphology, chip width and machining forces extracted from the FE machining simulations were compared against the experimental results in Tables 8, 9 and 10, specifically showing the SEM images of the chips reported by Yip and To [14] compared against the FEA models developed as part of this work. The comparative results show good proximity in the chip profile and cutting forces.

The large variations in chip width in combination 1 between analytical vs numerical and experiments suggest that the edges of chips were broken both in numerical and experimental results. This may be

Table 10

Comparison of simulated and experimental cutting forces for 2 μm, 4 μm and 7 μm depth of cut during machining of cast titanium alloy.

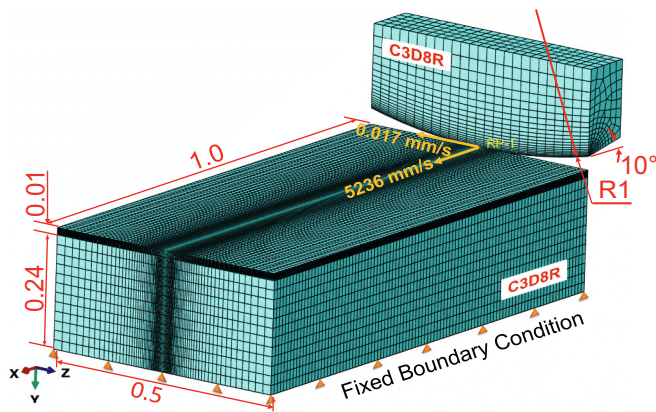| Combinations	Experimentally reported cutting forces while machining cast Ti6Al4V alloy by Yip and To [14]	Simulated cutting forces on cast Ti6Al4V alloy obtained in this work to validate the model
Combination 1: Speed: 25 mm/s, TFR: 0 mm/s, DOC: 1 μm		
Combination 2: Speed: 25 mm/s, TFR: 0 mm/s, DOC: 4 μm		
Combination 3: Speed: 25 mm/s, TFR: 0 mm/s, DOC: 7 μm		

Fig. 10. Meshed CAD geometries of the workpiece and tool mimicking the cutting process of Ti6Al4V using the experimental parameters during SPDM.

due to the low cutting depth at the edges resulting from nose radius. A slight variation in the error could be ascribed to the fact that the chip width measurements made in experiments are based on SEM images published previously which are not flat surfaces and have curly spatial components.

The magnitude of average cutting forces in both numerical simulations and experiments was found to be quite similar. The average cutting forces obtained during numerical simulation for 2 μm, 4 μm and 7 μm depth of cut were 0.7 N, 1.57 N and 3.2 N respectively against the experimental reported cutting forces of 0.7 N, 1.6 N and 3 N respectively.

4.2.2. FEA simulation of SPDM of Ti6Al4V and comparison with chip morphology of additively manufactured samples

A convincing validation of the FEA simulations with the reported data in the literature obtained in the previous section indicates that the model is fully predictive. Accordingly, we deployed the same model to simulate the cutting process that we had studied experimentally to assess whether the unique morphology of the cutting chips with intermittent fracture can be obtained. The CAD dimension of the model was appropriately adjusted to 1.0 × 0.5 × 0.25 mm to facilitate higher cutting speed of 5236 mm/s along the cutting direction and a secondary speed of 0.017 mm/s was prescribed for the tool motion along the feed direction (see Fig. 10).
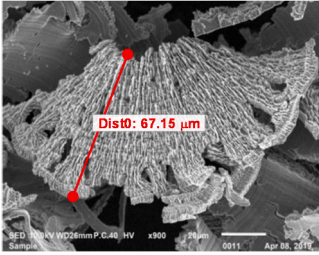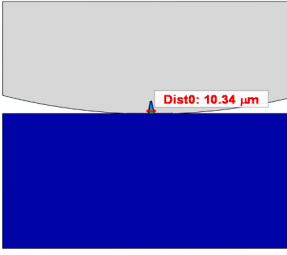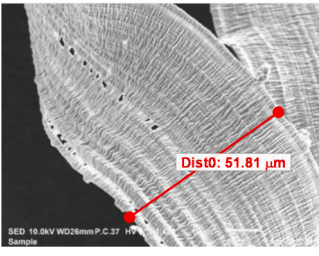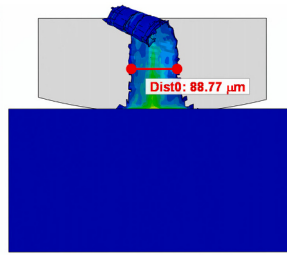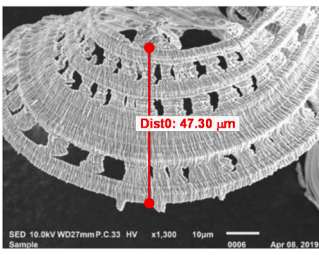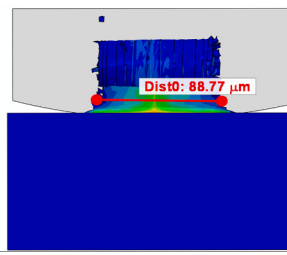
A comparison of the chip morphology obtained during the experiments and from the FEA model is shown in Table 11. These results showed significant differences in the chip widths and the chip morphology. The only difference between the prior results and this FEA model is the nature of the workpiece. Whereas the validation was based on cast Ti6Al4V alloys, our study used additively manufactured Ti6Al4V alloys. These two forms differ substantially in microstructure. Notably, as the depth of cut increased, the chip width decreased, a unique trend observed during the cutting of additively manufactured Ti6Al4V alloy as opposed to a cast Ti6Al4V alloy.

One can argue that the chips collected and measured from SEM were a result of successive machining cuts which are affected by the feed rate, whereas in FEA numerical calculations the chip widths were obtained after a single machining pass. However, we note that the same numerical model showed a good correlation during comparison of chip width with the published literature on cast Ti6Al4V alloys. Therefore, this consideration can be ruled out. Evidently, the mechanism of machining of additively manufactured Ti6Al4V alloys differs substantially from the machining mechanism and the allied theories proposed on metal machining thus far. This difference suggests the need for the development of newer models to explain the machining mechanics of additively manufactured parts.

It has already been stated that parameters such as laser power, hatch size, laser scan speed and quality of the powder have a significant impact on the parts produced by additive manufacturing. Due to discrete

Table 11

Comparison of experimental chip widths for depth of cuts of 1 μm, 5 μm and 10 μm obtained from the simulation of cutting of Ti6Al4V machining conditions.

	Chip width obtained from SPDM on additively manufactured Ti6Al4V alloys	Chip width obtained from FEA using traditional material constitutive model
Combination1: Speed: 2000 rpm TFR: 1 mm/min, DOC: 1 μm	Dist0: 67.15 μm	Dist0: 10.34 μm
Combination2: Speed: 2000 rpm, TFR: 3 mm/min, DOC: 5 μm	Dist0: 51.81 μm	Dist0: 88.77 μm
Combination3: Speed: 2000 rpm, TFR: 5 mm/min, DOC: 10 μm	Dist0: 47.30 μm	Dist0: 88.77 μm

heating and cooling rates in various locations, the notable mechanical and microstructural features of titanium alloy produced by additive manufacturing that are impacted are hardness, tensile strength, and non-homogenous density. Layer by layer material addition also induces porosity and brittleness to the part. Therefore, for a well-aligned computational simulation, it is necessary to devise a tailor-made material model, inclusive of material flow and damage properties, specifically for the FEM model aligned for the additively manufactured titanium alloy under specified process conditions. This may well need to obtain experimental properties of additively manufactured parts to inform the FEA model to obtain robust results. In recent times, it can be seen that researchers are attempting to use dislocation density-based theory to model the cutting behaviour of additively manufactured alloy, however, clearly, none of the existing models can describe the mechanism of chip formation in additively manufactured parts in sufficient detail as yet.

5. Conclusions

In our detailed investigation on the SPDM of additively manufactured Ti6Al4V ELI alloy, we observed several key differences compared to established results obtained from cast alloys. Notably, the relationship between feed rate and surface roughness in our experiments challenged traditional understanding in the machining domain, i.e., we noticed that an increasing feed rate surprisingly led to an improved machined surface (reduced roughness) in the case of additively manufactured alloy. This variation can be attributed, in part, to the unique chip morphologies we observed, which have not been reported previously in the literature of machining additively made materials.

Furthermore, our experiments highlighted the nuanced role of tool geometry in machining performance. Tools featuring a smaller nose radius of 1 mm consistently delivered superior results, emphasizing the need to carefully consider tool specifications when machining additively manufactured materials. Our FEA simulations, initially validated against published literature on cast alloys, seemed promising in their predictive capabilities. However, when these same models were adapted to our study's unique conditions, they showed clear discrepancies. These discrepancies suggest that differences exist in machining mechanics between additively manufactured and cast Ti6Al4V alloys. We acknowledge simplified assumptions used in the model development, however while the same model showed good predictability with the cast alloys, it showed no proximity when extended to predict the machining outcome of the additively made Ti6Al4V alloys. The overarching influence of microstructure on machining outcomes is evidenced in our study underscore a pressing requirement in the machining community: the need for more specialized models that can cater to the complexities inherent in machining additively manufactured alloys. In sum, the main takeaway from our work is that the structure of a material, especially how it is made, can change how it behaves when being machined, even if the alloy is the same. As more materials are developed through additive manufacturing, we need to develop more robust computer models (based on the additive manufacturing process parameters) to obtain accurate machining results.

Declaration of competing interest

The authors declare that they have no known competing financial interests or personal relationships that could have appeared to influence the work reported in this paper.

Appendix A. Supplementary data

Supplementary data to this article can be found online at https://doi.org/10.1016/j.jmapro.2024.04.051.

References

[1] Zhang T, Liu C-T. Design of titanium alloys by additive manufacturing: a critical review. Advanced Powder Materials 2022;1:100014.

[2] DebRoy T, Wei H, Zuback J, Mukherjee T, Elmer J, Milewski J, Beese AM. Additive manufacturing of metallic components–process, structure and properties. Progress in Materials Science 2018;92:112–224.

[3] Manjunath K, Tewary S, Khatri N, Cheng K. Precipitation effect on surface roughness at Ti-6Al-4 V ELI alloy during ultra-precision machining. International Journal on Interactive Design and Manufacturing 2022;IJIDeM:1–9.

[4] Ni J, Ling H, Zhang S, Wang Z, Peng Z, Benyshek C, et al. Three-dimensional printing of metals for biomedical applications. Materials Today Bio 2019;3: 100024.

[5] Rack H, Qazi J. Titanium alloys for biomedical applications. Mater Sci Eng C 2006; 26:1269–77.

[6] Vayssette B, Saintier N, Brugger C, Elmay M, Pessard E. Surface roughness of Ti-6Al-4V parts obtained by SLM and EBM: effect on the high cycle fatigue life. Procedia engineering 2018;213:89–97.

[7] Ni C, Zhu L, Zheng Z, Zhang J, Yang Y, Yang J, et al. Effect of material anisotropy on ultra-precision machining of Ti-6Al-4V alloy fabricated by selective laser melting. J Alloys Compd 2020;848:156457.

[8] Hojati F, Daneshi A, Soltani B, Azarhoushang B, Biermann D. Study on machinability of additively manufactured and conventional titanium alloys in micro-milling process. Precis Eng 2020;62:1–9.

[9] Ostra T, Alonso U, Veiga F, Ortiz M, Ramiro P, Alberdi A. Analysis of the machining process of inconel 718 parts manufactured by laser metal deposition. Materials 2019;12:2159.

[10] Oyelola O, Crawforth P, M'Saoubi R, Clare AT. Machining of additively manufactured parts: implications for surface integrity. Procedia Cirp 2016;45: 119–22.

[11] Le Coz G, Fischer M, Piquard R, D'acunto A, Laheurte P, Dudzinski D. Micro cutting of Ti-6Al-4V parts produced by SLM process. Procedia Cirp 2017;58:228–32.

[12] Goel S, Luo X, Reuben RL. Molecular dynamics simulation model for the quantitative assessment of tool wear during single point diamond turning of cubic silicon carbide. Comput Mater Sci 2012;51:402–8.

[13] Ruibin X, Wu H. Study on cutting mechanism of Ti6Al4V in ultra-precision machining. The International Journal of Advanced Manufacturing Technology 2016;86:1311–7.

[14] Yip W, S. To. Ductile and brittle transition behavior of titanium alloys in ultra-precision machining. Sci Rep 2018;8:1–8.

[15] Goel S, Luo X, Comley P, Reuben RL, Cox A. Brittle–ductile transition during diamond turning of single crystal silicon carbide. Int J Mach Tool Manuf 2013;65: 15–21.

[16] Colafemina JP, Jasinevicius RG, Duduch JG. Surface integrity of ultra-precision diamond turned Ti (commercially pure) and Ti alloy (Ti-6Al-4V). Proceedings of the Institution of Mechanical Engineers, Part B: Journal of Engineering Manufacture 2007;221:999–1006.

[17] Chauhan S, Dass K. Optimization of machining parameters in turning of titanium (grade-5) alloy using response surface methodology. Materials and manufacturing processes 2012;27:531–7.

[18] Ramesh S, Karunamoorthy L, Palanikumar K. Measurement and analysis of surface roughness in turning of aerospace titanium alloy (gr5). Measurement 2012;45: 1266–76.

[19] Heidari M, Yan J. Nanometer-scale chip formation and surface integrity of pure titanium in diamond turning. The International Journal of Advanced Manufacturing Technology 2018;95:479–92.

[20] Zhang Y, Zhou Z, Wang J, Li X. Diamond tool wear in precision turning of titanium alloy. Materials and Manufacturing Processes 2013;28:1061–4.

[21] Minton T, Ghani S, Sammler F, Bateman R, Fürstmann P, Roeder M. Temperature of internally-cooled diamond-coated tools for dry-cutting titanium. Int J Mach Tool Manuf 2013;75:27–35.

[22] Yip W, S. To. An application of eddy current damping effect on single point diamond turning of titanium alloys. J Phys D Appl Phys 2017;50:435002.

[23] Revankar GD, Shetty R. Response surface model for surface roughness during finish turning of titanium alloy under minimum quantity lubrication. In: International Conference on Emerging Trends in Engineering and Technology (ICETET'2013) at: Patong Beach, Phuket (Thailand); 2013. p. 78–84.

[24] Lou Y, Chen L, Wu H, S. To. Influence of cutting velocity on surface roughness during the ultra-precision cutting of titanium alloys based on a comparison between simulation and experiment. PloS One 2023;18:e0288502.

[25] Obikawa T, Usui E. Computational machining of titanium alloy—finite element modeling and a few results 1996;118(2):208–15.

[26] Vijay Sekar K, Pradeep Kumar M. Finite element simulations of Ti6Al4V titanium alloy machining to assess material model parameters of the Johnson-cook constitutive equation. Journal of the Brazilian Society of Mechanical Sciences and Engineering 2011;33:203–11.

[27] Styger G, Laubscher RF, Oosthuizen GA. Effect of constitutive modeling during finite element analysis of machining-induced residual stresses in Ti6Al4 V. Procedia CIRP 2014;13:294–301.

[28] Hall S, Loukaides E, Newman ST, Shokrani A. Computational and experimental investigation of cutting tool geometry in machining titanium Ti-6Al-4V. Procedia CIRP 2019;86:139–44.

[29] Jagadesh T, Samuel G. Finite element simulations of micro turning of Ti-6Al-4V using PCD and coated carbide tools. Journal of The Institution of Engineers (India): Series C 2017;98:5–15.

[30] Reddy MM, Kumar M, Shanmugam K. Finite element analysis and modeling of temperature distribution in turning of titanium alloys. Metallurgical and Materials Engineering 2018;24:59–69.

[31] Lou Y, Wu H. Improving machinability of titanium alloy by electro-pulsing treatment in ultra-precision machining. The International Journal of Advanced Manufacturing Technology 2017;93:2299–304.

[32] Mir A, Luo X, Llavori I, Roy A, Zlatanovic DL, Joshi SN, et al. Challenges and issues in continuum modelling of tribology, wear, cutting and other processes involving high-strain rate plastic deformation of metals. J Mech Behav Biomed Mater 2022; 105185.

[33] Liu C, Goel S, Llavori I, Stolf P, Giusca CL, Zabala A, et al. Benchmarking of several material constitutive models for tribology, wear, and other mechanical deformation simulations of Ti6Al4V. J Mech Behav Biomed Mater 2019;97: 126–37.

[34] Kumar M, Meena VK, Singh S. Static and fatigue load bearing investigation on porous structure titanium additively manufactured anterior cervical cages. Biomed Res Int 2022;2022.

[35] V.K. Meena, P. Kumar, T. Panchal, P. Kalra, R.K. Sinha, Investigation of Titanium Lattice Structures for Biomedical Implants, in: Advanced Materials for Biomedical Applications, CRC Press, pp. 159–168.

[36] Meena VK, Kumar P, Kalra P, Sinha RK. Additive manufacturing for metallic spinal implants: a systematic review, annals of 3D. Printed Medicine 2021;3:100021.

[37] Li Z, Kucukkoc I, Zhang DZ, Liu F. Optimising the process parameters of selective laser melting for the fabrication of Ti6Al4V alloy. Rapid Prototyping Journal 2018; 24(1):150–9.

[38] Meena VK, Kalra P, Sinha RK. Additive manufacturing parameters optimization of Ti6AL4V Eli for medical implants. Surface Review and Letters 2022;29:2250040.

[39] Manjunath K, Tewary S, Khatri N, Cheng K. Simulation-based investigation on ultra-precision machining of additively manufactured Ti-6Al-4V ELI alloy and the associated experimental study. Proceedings of the Institution of Mechanical Engineers, Part B: Journal of Engineering Manufacture 2023;0(0). https://doi.org/10.1177/09544054231196920.

[40] Wang H, S. To, Chan C, Cheung CF, Lee WB. A theoretical and experimental investigation of the tool-tip vibration and its influence upon surface generation in single-point diamond turning. Int J Mach Tool Manuf 2010;50:241–52.

[41] Yip W, S. To. Reduction of material swelling and recovery of titanium alloys in diamond cutting by magnetic field assistance. J Alloys Compd 2017;722:525–31.

[42] Wang Y, Zou B, Wang J, Wu Y, Huang C. Effect of the progressive tool wear on surface topography and chip formation in micro-milling of Ti–6Al–4V using Ti (C7N3)-based cermet micro-mill. Tribology International 2020;141:105900.

[43] Khatri N, Barkachary BM, Muneeswaran B, Al-Sayegh R, Luo X, Goel S. Surface defects incorporated diamond machining of silicon. International Journal of Extreme Manufacturing 2020;2:045102.

[44] Mariayyah R. Experimental and numerical studies on ductile regime machining of silicon carbide and silicon nitride. The University of North Carolina at Charlotte; 2007.

[45] Chen G, Ren C, Yang X, Jin X, Guo T. Finite element simulation of high-speed machining of titanium alloy (Ti–6Al–4V) based on ductile failure model. The International Journal of Advanced Manufacturing Technology 2011;56:1027–38.

[46] Liu S. FEM simulation and experiment research of cutting temperature and force in orthogonal cutting of titanium alloys. Master's thesis of Nanjing University of Aeronautics & Astronautics 2007;1.

[47] Sun J, Guo Y. Material flow stress and failure in multiscale machining titanium alloy Ti-6Al-4V. The International Journal of Advanced Manufacturing Technology 2009;41:651–9.